ELSEVIER

International Journal of Solids and Structures 41 (2004) 5051–5069

INTERNATIONAL JOURNAL OF SOLIDS and STRUCTURES

www.elsevier.com/locate/ijsolstr

Wave propagation in a hollow cylinder due to prescribed velocity at the boundary

Michael El-Raheb *

Wave Research, Applied Mechanics, 1000 Oak Forest Lane, Pasadena, CA 91107, USA

Received 6 January 2004; received in revised form 7 April 2004
Available online 6 May 2004

Abstract

Analyzed is transient response of a hollow cylinder to time dependent radial and axial velocities prescribed at the cylinder's inner boundary. Modal and static solutions are superimposed for solving transient response. Axial dependence is expressed by two orthogonal sets of periodic functions; one set satisfies vanishing axial stress at the cylinder ends and applies to the radial traction problem, and the other set satisfies vanishing shear stress at the ends and applies to the axial traction problem. The mixed boundary value problem with velocity prescribed over part of the boundary and vanishing stress prescribed over the remaining part is analyzed by the method of influence coefficients. This method superimposes response from several external annular traction segments of unit intensity with time dependent weights yielding a combined response equal to the prescribed instantaneous velocity.

Keywords: Wave propagation; Transient response; Concentric cylinder; Mixed boundary value problem; Influence coefficients

1. Introduction

Trauma in human organs from projectile penetration is caused by two mechanisms:

(i) Tissue damage along projectile path. This interaction is hydrodynamic in nature where inertial and frictional forces dominate the projectile's motion as it decelerates and eventually stops.
(ii) Stress waves generated at the cylindrical interface between projectile and tissue from radial and axial velocities prescribed by the projectiles during penetration. These waves radiate to neighboring tissue and organs causing further damage.

The present analysis concerns mechanism (ii) above.

* Tel.: +1-626-7965528; fax: +1-626-5838834.
E-mail address: mertrident@earthlink.net (M. El-Raheb).

0020-7683/$ - see front matter © 2004 Elsevier Ltd. All rights reserved.
doi:10.1016/j.ijsolstr.2004.04.016

As the projectile penetrates into tissue, it moves material by replacing it with its own volume. When the material fails, it acts more like a fluid, lessening the amount of material being compressed. In the radial direction, material is compressed by an expanding cross-section of the projectile's smoothly curved nose. As long as the projectile's speed is much smaller than the speed of stress waves in the material, the moving projectile can be approximated by radial and axial velocities prescribed along its boundary. For a projectile speed of 330 ft/s and a dilatational speed in tissue material of 5600 ft/s, this approximation is valid.

Dynamic response of solid and hollow elastic cylinders has been studied extensively in the literature as it applies to a variety of engineering and science problems. A large body of references concerns sound scattering by elastic cylinders in the frequency domain. Among these are Stanton (1988), Honarvar and Sinclair (1996), Bao et al. (1997), Wang and Ying (2001). Stepanishen and Janus (1990) treat transient radiation and scattering from fluid loaded cylinders. Frequency response of cylinders is analyzed by Grinchenko and Meleshko (1978), Batard and Quentin (1992), and Grinchenko (1999). Soldatos and Ye (1994) treat anisotropic laminated cylinders, and Hussein and Heyliger (1998) consider layered piezoelectric cylinders. Cheung et al. (2003) analyze the 3-D vibration of solid and hollow cylinders by the Chebyshev–Ritz method. Very few references discuss transient response of elastic cylinders. Paul and Murali (1995) determine the axisymmetric dynamic response of poro-elastic cylinders. Soldatos (1994) presents a compilation of more than 150 references on frequency response of solid and annular elastic cylinders, yet not a single one addresses transient response. Yin and Yue (2002) solve the transient plane-strain response from impulse of infinite length multi-layered cylinders. From the list above, this is the only reference relevant to a special case of the present analysis.

The influenced region is simulated by tissue material in the shape of a hollow cylinder. Let (r,z) be radial and axial coordinates with origin at one end of the cylinder axis. The inner cylinder radius r_{p} is that of the penetrating projectile while its outer radius r_{o} and length l are chosen to include the furthest radial and axial locations affected by penetration. In a coordinate system (r,z) centered at one end of the finite cylinder, the projectile lies in the interval $z_a \leqslant z \leqslant z_b$ such that $z_b - z_a = l_{\mathrm{p}}$ where l_{p} is projectile length. The tissue material is linear visco-elastic with a constitutive law that includes first temporal derivatives of stress and strain.

For simplicity and without loss of generality, axial functions satisfying the differential equations and specific boundary conditions at the two ends of the cylinder $z = (0, l)$ are divided into 2 sets. One set satisfying vanishing axial stress σ_{zz} at $z = (0, l)$ which has radial and axial displacements (u, w) proportional to $(\sin(m\pi z/l), \cos(m\pi z/l))$ belongs to "problem 1", where m is an integer wave number. The other set satisfying vanishing shear stress τ_{rz} at $z = (0, l)$ which has (u, w) proportional to $(\cos(m\pi z/l), \sin(m\pi z/l))$ belongs to "problem 2". The first set applies to radial tractions prescribed at the cylindrical footprint $r = r_{\mathrm{o}}$, $z_a \leqslant z \leqslant z_b$ while the second set applies to prescribed axial tractions along the same footprint. The fact that each set satisfies different boundary conditions does not affect transient response until waves reflect from the axial boundaries. Consequently, one problem is solved for each type of forcing excitation and results are superimposed if both types of excitation are acting simultaneously.

The form of the forcing function closest to the application is radial and axial velocity prescribed over part of the inner cylindrical boundary, yet this leads to a mixed boundary condition. This difficulty can be overcome by superimposing response from a set of unit radial or axial tractions with time dependent weights prescribed on annular portions of the inner boundary. These weights are updated at each time step using the condition that combined velocity response at the center of each annular portion equals the prescribed instantaneous velocity. In this way, the forcing function is converted to pure radial or axial traction with time varying spatial dependence.

Section 2 derives frequency and transient response of the hollow cylinder with finite length. Section 3 presents stress histories from prescribed radial and axial pressures and velocities at the inner boundary.

1.1. Elastic analysis

In the analysis to follow, all subscripts will denote components and not partial derivatives. In cylindrical coordinates, the elastodynamic equations are

$$\begin{aligned}&\mu\nabla^2\mathbf{u}+(\lambda+\mu)\nabla(\nabla\cdot\mathbf{u})=\rho\partial_{tt}\mathbf{u}\\&\nabla^2\equiv\partial_{rr}+1/r\partial_r+1/r^2\partial_{\theta\theta}+\partial_{zz}\\&\nabla\equiv(1/r\partial_r r)\mathbf{e}_r+(1/r\partial_\theta)\mathbf{e}_\theta+(\partial_z)\mathbf{e}_z\end{aligned}\tag{1}$$

(r,θ,z) are radial, circumferential and axial independent variables, $\mathbf{u}=\{u,v,w\}^{\mathrm{T}}$ is displacement vector along these directions, (λ,μ) are Lame constants, ρ is mass density and t is time. Re-write (1) as

$$\mu\nabla^2\mathbf{u}+(\lambda+2\mu)\nabla(\nabla\cdot\mathbf{u})-\mu\nabla(\nabla\cdot\mathbf{u})=\rho\partial_{tt}\mathbf{u}\tag{2a}$$

Noting that

$$\mu\nabla^2\mathbf{u}-\mu\nabla(\nabla\cdot\mathbf{u})=-\mu\nabla\times\nabla\times\mathbf{u}\tag{2b}$$

permits casting (1) in the form

$$(\lambda+2\mu)\nabla(\nabla\cdot\mathbf{u})-\mu\nabla\times\nabla\times\mathbf{u}=\rho\partial_{tt}\mathbf{u}\tag{3}$$

Define dilatation Δ and rotation vector $\boldsymbol{\psi}$ as

$$\Delta=\nabla\cdot\mathbf{u},\quad\boldsymbol{\psi}=\nabla\times\mathbf{u}\tag{4}$$

Substituting (4) in (3) yields (Love, 1944)

$$(\lambda+2\mu)\nabla\Delta-\mu\nabla\times\boldsymbol{\psi}=\rho\partial_{tt}\mathbf{u}\tag{5}$$

Taking the divergence of (5) noting that $\nabla\cdot(\nabla\times\boldsymbol{\psi})=0$ yields

$$(\lambda+2\mu)\nabla^2\Delta=\rho\Delta_{tt}\tag{6}$$

Taking the rotation of (5) noting that $\nabla\times(\nabla\Delta)=0$ yields

$$\mu\nabla^2\boldsymbol{\psi}=\rho\boldsymbol{\psi}_{tt}\tag{7}$$

For axisymmetric motions, $v\equiv\partial_\theta\equiv 0$ and $\psi_r\equiv\psi_z\equiv 0$ reducing (6) and (7) to

$$\begin{aligned}&(\lambda+2\mu)\nabla_0^2\Delta=\rho\Delta_{tt}\\&\mu\nabla_1^2\psi_\theta=\rho\psi_{\theta,tt}\\&\nabla_n^2\equiv\partial_{rr}+1/r\partial_r-n^2/r^2+\partial_{zz},\quad n=0,1\end{aligned}\tag{8}$$

Expressing (4) in terms of $\mathbf{u}$ yields

$$\begin{aligned}&\Delta=1/r\partial_r(ru)+\partial_z w\\&\psi_\theta=\partial_z u-\partial_r w\end{aligned}\tag{9}$$

Decoupling u and w in (9) produces

$$\begin{aligned}&\nabla_1^2u=\partial_r\Delta+\partial_z\psi_\theta\\&\nabla_0^2w=\partial_z\Delta-1/r\partial_r(r\psi_\theta)\end{aligned}\tag{10}$$

For the radial "problem 1" satisfying $\sigma_{zz}=0$ at $z=(0,l)$, harmonic motions in time with radian frequency ω and simply supported boundaries at $z=(0,l)$ yields the separated solution

$$\begin{aligned}\{\Delta(r,z,t),\psi_\theta(r,z,t)\}^{\mathrm{T}} &= \{\overline{\Delta}(r)\cos(k_z z),\overline{\psi}_\theta(r)\sin(k_z z)\}^{\mathrm{T}}\mathrm{e}^{\mathrm{i}\omega t}\\ \{u(r,z,t),w(r,z,t)\}^{\mathrm{T}} &= \{\bar{u}(r)\sin(k_z z),\bar{w}(r)\cos(k_z z)\}^{\mathrm{T}}\mathrm{e}^{\mathrm{i}\omega t}\end{aligned} \tag{11}$$

$\mathrm{i}=\sqrt{-1}$ and $k_z = m\pi/l$ where m is an integer axial wave number. The z dependence in (11) yields $u=\sigma_{zz}=0$ at the cylinder ends $z=0,l$. For real k_e and k_s, Eq. (8) admits the solution

$$\begin{aligned}\overline{\Delta}(r) &= C_1 J_0(k_e r)+C_2 Y_0(k_e r)\\ \bar{\psi}_\theta(r) &= C_3 J_1(k_s r)+C_4 Y_1(k_s r)\end{aligned} \tag{12}$$

$$k_e^2=\omega^2/c_{\mathrm{d}}^2-k_z^2,\quad c_{\mathrm{d}}^2=(\lambda+2\mu)/\rho$$

$$k_s^2=\omega^2/c_{\mathrm{s}}^2-k_z^2,\quad c_{\mathrm{s}}^2=\mu/\rho$$

J_n and Y_n are Bessel functions and $c_{\mathrm{d}}, c_{\mathrm{s}}$ are dilatational and shear speeds of sound. If either k_e or k_s is imaginary, J_n and Y_n in (12) are replaced by the modified Bessel functions I_n and K_n with appropriate changes in sign. Substituting (11) and (12) in (10) then solving for $\bar{u}(r)$ and $\bar{w}(r)$ yields

$$\begin{aligned}\bar{u}(r) &= -k_e(C_1J_1(k_e r)+C_2Y_1(k_e r))+k_z(C_3J_1(k_s r)+C_4Y_1(k_s r))\\ \bar{w}(r) &= k_z(C_1J_0(k_e r)+C_2Y_0(k_e r))+k_s(C_3J_0(k_s r)+C_4Y_0(k_s r))\end{aligned} \tag{13}$$

In cylindrical coordinates, the constitutive relations are

$$\begin{aligned}&\sigma_{rr}=\lambda\Delta+2\mu\partial_r u,\quad \sigma_{\theta\theta}=\lambda\Delta+2\mu u/r\\ &\sigma_{zz}=\lambda\Delta+2\mu\partial_z w,\quad \tau_{rz}=\mu(\partial_z u+\partial_r w)\\ &\Delta=\partial_r u+u/r+\partial_z w\end{aligned} \tag{14}$$

For "problem 1", harmonic motions in time and simply supported boundaries at $(0,l)$ yield the separated relations

$$\begin{Bmatrix}\sigma_{rr}\\ \sigma_{\theta\theta}\\ \sigma_{zz}\\ \tau_{rz}\end{Bmatrix}(r,z,t)=\begin{Bmatrix}\bar{\sigma}_{rr}(r)\sin(k_z z)\\ \bar{\sigma}_{\theta\theta}(r)\sin(k_z z)\\ \bar{\sigma}_{zz}(r)\sin(k_z z)\\ \bar{\tau}_{rz}(r)\cos(k_z z)\end{Bmatrix}\mathrm{e}^{\mathrm{i}\omega t} \tag{15a}$$

Boundary conditions at $r=r_{\mathrm{p}}$ and $r=r_{\mathrm{o}}$ are

$$\begin{aligned}&\sigma_{rr}(r_{\mathrm{p}},z,t)=p_r(t)[H(z-z_a)-H(z-z_b)]\\ &\tau_{rz}(r_{\mathrm{p}},z,t)=0\\ &\sigma_{rr}(r_{\mathrm{o}},z,t)\equiv\tau_{rz}(r_{\mathrm{o}},z,t)=0\end{aligned} \tag{15b}$$

$p_r(t)$ is a time dependent uniform radial traction acting on the inner cylindrical boundary $r=r_{\mathrm{p}}$ in the interval $z_a\leqslant z\leqslant z_b$. The z dependence in (15a) yields $u=\sigma_{zz}=0$ at the cylinder ends $z=0,l$. Substituting (11), (13) and (15a) in (14) yields

$$\begin{aligned}\bar{\sigma}_{rr}(r) &= \big[-\big((\lambda+2\mu)k_e^2+\lambda k_z^2\big)J_0(k_e r)+2\mu k_e^2 J_1(k_e r)/(k_e r)\big]C_1\\ &\quad+\big[-\big((\lambda+2\mu)k_e^2+\lambda k_z^2\big)Y_0(k_e r)+2\mu k_e^2 Y_1(k_e r)/(k_e r)\big]C_2\\ &\quad+2\mu k_s k_z[J_0(k_s r)-J_1(k_s r)/(k_s r)]C_3+2\mu k_s k_z[Y_0(k_s r)-Y_1(k_s r)/(k_s r)]C_4\end{aligned} \tag{16a}$$

$$\begin{aligned}\bar{\sigma}_{\theta\theta}(r) &= -\big[\lambda(k_z^2+k_e^2)J_0(k_e r)+2\mu k_e^2 J_1(k_e r)/(k_e r)\big]C_1\\ &\quad-\big[\lambda(k_z^2+k_e^2)Y_0(k_e r)+2\mu k_e^2 Y_1(k_e r)/(k_e r)\big]C_2+2\mu k_s k_z[C_3J_1(k_s r)+C_4Y_1(k_s r)]/(k_s r)\end{aligned} \tag{16b}$$

$$\bar{\sigma}_{zz}(r) = -\left((\lambda+2\mu)k_z^2 + \lambda k_e^2\right)[C_1 J_0(k_e r) + C_2 Y_0(k_e r)] - 2\mu k_s k_z [C_3 J_0(k_s r) + C_4 Y_0(k_s r)] \tag{16c}$$

$$\bar{\tau}_{rz}(r) = -2\mu k_e k_z [C_1 J_1(k_e r) + C_2 Y_1(k_e r)] - \mu(k_s^2 - k_z^2)[C_3 J_1(k_s r) + C_4 Y_1(k_s r)] \tag{16d}$$

Since σ_{zz} is proportional to $\sin(k_z z)$ in (15), it vanishes at $z = 0, l$. This allows a rigid body motion $w(r,z;t) = w_o(t)$ when external traction acts along z. To avoid the rigid body motion, an additional axial functional dependence is considered for "problem 2"

$$\begin{Bmatrix} u \\ w \end{Bmatrix}(r,z,t) = \begin{Bmatrix} \bar{u}(r)\cos(k_z z) \\ \bar{w}(r)\sin(k_z z) \end{Bmatrix} e^{i\omega t}$$
$$\begin{Bmatrix} \sigma_{rr} \\ \sigma_{\theta\theta} \\ \sigma_{zz} \\ \tau_{rz} \end{Bmatrix}(r,z,t) = \begin{Bmatrix} \bar{\sigma}_{rr}(r)\cos(k_z z) \\ \bar{\sigma}_{\theta\theta}(r)\cos(k_z z) \\ \bar{\sigma}_{zz}(r)\cos(k_z z) \\ \bar{\tau}_{rz}(r)\sin(k_z z) \end{Bmatrix} e^{i\omega t} \tag{17a}$$

that satisfies the following boundary conditions at $r = r_p$ and $r = r_o$

$$\begin{aligned} &\sigma_{rr}(r_p,z,t) = 0 \\ &\tau_{rz}(r_p,z,t) = p_z(t)[H(z-z_a) - H(z-z_b)] \\ &\sigma_{rr}(r_o,z,t) \equiv \tau_{rz}(r_o,z,t) = 0 \end{aligned} \tag{17b}$$

$p_z(t)$ is a time dependent uniform axial traction acting on the inner cylindrical boundary $r = r_p$ in the interval $z_a \leqslant z \leqslant z_b$. The z dependence in (18a) yields $w = \tau_{rz} = 0$ at the cylinder ends $z = 0, l$. In the analysis to follow, superscripts (1) and (2) will denote radial and axial problems respectively. Derivations for problem (2) follow the same steps as those for problem (1) and are omitted here for shortness. Although conditions at the boundaries $z = 0, l$ of each problems are different, they do not affect the transient response at times preceding reflection of waves from these boundaries.

Divide the cylindrical surface $\{r = r_p, z_a \leqslant z \leqslant z_b\}$ into $n+1$ equidistant ring stations with increment Δz_p

$$\begin{aligned} &z_1, z_2, z_3, \ldots, z_n, \quad z_l - z_{l-1} = \Delta z_p = \text{const} \\ &z_l = z_a + (l-1)\Delta z_p \end{aligned} \tag{18}$$

Assume a uniform pressure of unit intensity to act over each ring segment $z_{l-1} \to z_l$. The elasto-dynamic solution to the kth ring pressure segment is outlined below.

For each pressure segment, expand each dependent variable in terms of eigenfunctions that satisfy homogeneous boundary conditions. Express total displacement $\mathbf{u}_k(r,z;t)$ as a superposition of two terms

$$\mathbf{u}_k^{(1,2)}(r,z;t) = \mathbf{u}_{sk}^{(1,2)}(r,z) f_p(t) + \mathbf{u}_{dk}^{(1,2)}(r,z;t) \tag{19}$$

$\mathbf{u}_{sk}^{(1,2)}(r,z)$ is static displacement vector satisfying (2a) when time derivative vanishes (Appendix A), $\mathbf{u}_{dk}^{(1,2)}(r,z;t)$ is dynamic displacement vector satisfying the dynamic equation of motion (2a), and $f_p(t)$ is time dependence of the forcing pressure. For each axial wave number m, express $\mathbf{u}_{dk}^{(1,2)}(r,z,t)$ in the eigenfunctions $\mathbf{\Phi}_{mj}^{(1,2)}(r,z)$ (Appendix B)

$$\mathbf{u}_{dk}^{(1,2)}(r,z,t) = \sum_j \sum_m a_{mjk}^{(1,2)}(t)\mathbf{\Phi}_{mj}^{(1,2)}(r,z) \tag{20}$$

$a_{mjk}^{(1,2)}(t)$ is a generalized coordinate of the jth eigenfunction with m axial half waves from the kth pressure segment. Substituting (19) and (20) in (2a) and enforcing orthogonality of $\mathbf{\Phi}_{mj}^{(1,2)}(r,z)$ yields uncoupled equations in $a_{mjk}^{(1,2)}(t)$. For an undamped elastic cylinder the equation governing $a_{mjk}^{(1,2)}(t)$ is

$$\left(\frac{\mathrm{d}^2}{\mathrm{d}t^2}+\omega_{mj}^2\right)a_{mjk}^{(1,2)}(t)=\bar{f}_{mjk}^{(1,2)}(t) \tag{21a}$$

$$\begin{aligned}
&\bar{f}_{mjk}^{(1,2)}(t)=N_{amjk}^{(1,2)}\ddot{f}_p(t)/N_{mj}\\
&N_{mj}^{(1,2)}=\int_0^{r_\mathrm{d}}\int_0^{h}\mathbf{\Phi}_{mj}^{(1,2)}(r,z)\cdot\mathbf{\Phi}_{mj}^{(1,2)}(r,z)\,\mathrm{d}z\,r\,\mathrm{d}r\\
&N_{amjk}^{(1,2)}=\int_0^{r_\mathrm{d}}\int_0^{h}\mathbf{u}_{sk}^{(1,2)}(r,z)\cdot\mathbf{\Phi}_{mj}^{(1,2)}(r,z)\,\mathrm{d}z\,r\,\mathrm{d}r
\end{aligned} \tag{21b}$$

ω_{mj} is the resonant frequency. The solution to (21a) takes the form

$$a_{mjk}^{(1,2)}(t)=-\frac{1}{\omega_{mj}}\int_0^t\sin\omega_{mj}(t-\tau)\bar{f}_{mjk}^{(1,2)}(\tau)\,\mathrm{d}\tau \tag{22}$$

Evaluating radial and axial displacements $u_k(r,z;t)$ for problem (1) and $w_k(r,z;t)$ for problem (2) from the kth pressure segment at each central point $z_{\mathrm{c}l}=(z_l+z_{l-1})/2$ of a pressure segment yields coefficients of the influence matrices

$$\begin{aligned}
U_{lk}(t)&=\sum_j\sum_m a_{mjk}^{(1)}(t)\bar{u}_{mjk}^{(1)}(r_\mathrm{p},z_{\mathrm{c}l})+u_{sk}^{(1)}(r_\mathrm{p},z_{\mathrm{c}l})f_p(t)\\
W_{lk}(t)&=\sum_j\sum_m a_{mjk}^{(2)}(t)\bar{w}_{mjk}^{(2)}(r_\mathrm{p},z_{\mathrm{c}l})+w_{sk}^{(2)}(r_\mathrm{p},z_{\mathrm{c}l})f_p(t)
\end{aligned} \tag{23}$$

$\{\bar{u}_{mjk}^{(1)}(r_\mathrm{p},z_{\mathrm{c}l}),\ \bar{w}_{mjk}^{(2)}(r_\mathrm{p},z_{\mathrm{c}l})\}$ and $\{u_{sk}^{(1)}(r_\mathrm{p},z_{\mathrm{c}l}),\ w_{sk}^{(2)}(r_\mathrm{p},z_{\mathrm{c}l})\}$ are modal and static displacement dyads at $z_{\mathrm{c}l}$ from the kth pressure segment in problems (1) and (2) respectively. In (21) and (23) $f_p(t)$ is a first approximation to the time dependence of the applied pressure. One approximation is determined from the plane- strain state when axial length of cylinder and footprint approaches infinity (Appendix C). Enforcing the condition of prescribed displacements $u_\mathrm{p}^{(1)}(t)$ and $w_\mathrm{p}^{(2)}(t)$ at each time step yields a set of simultaneous equations in the weights $p_k^{(1)}$ and $p_k^{(2)}$

$$\begin{aligned}
&\sum_{k=1}^{n}U_{lk}(t)p_k^{(1)}(t)=u_\mathrm{p}^{(1)}(t),\quad l=1,\ldots,n\\
&\sum_{k=1}^{n}W_{lk}(t)p_k^{(2)}(t)=w_\mathrm{p}^{(2)}(t),\quad l=1,\ldots,n
\end{aligned} \tag{24}$$

In what follows, superscripts (1,2) are dropped for shortness. For an elastic material, eigenvalues and resonant frequencies are synonymous. In this case, the eigenvalues appear in pairs ω_{mj} and $-\omega_{mj}$. Consequently Eq. (22a) takes the form

$$\left(\frac{\mathrm{d}}{\mathrm{d}t}-\mathrm{i}\omega_{mj}\right)\left(\frac{\mathrm{d}}{\mathrm{d}t}+\mathrm{i}\omega_{mj}\right)a_{mjk}(t)=\bar{f}_{mjk}(t) \tag{25a}$$

$$\begin{aligned}
&\bar{f}_{mjk}(t)=N_{amjk}\ddot{f}_p(t)/N_{mj}\\
&N_{amjk}=\int_0^{l}\int_{r_\mathrm{p}}^{r_\mathrm{o}}u_{sk}(r,z)\cdot\mathbf{\Phi}_{mj}(x,z)r\,\mathrm{d}r\,\mathrm{d}z\\
&N_{mj}=\int_0^{l}\int_{r_\mathrm{p}}^{r_\mathrm{o}}\mathbf{\Phi}_{mj}(r,z)\cdot\mathbf{\Phi}_{mj}(r,z)r\,\mathrm{d}r\,\mathrm{d}z
\end{aligned} \tag{25b}$$

1.2. Visco-elastic analysis

For a visco-elastic material, ω_{mj} and $\mathbf{\Phi}_{mj}(r,z)$ in (25) are both complex

$$\omega_{mj} = \omega_{m\mathrm{R}j} + \mathrm{i}\omega_{m\mathrm{I}j} \tag{26a}$$

$$N_{mj} = \int_0^l \int_{r_\mathrm{p}}^{r_\mathrm{o}} \mathbf{\Phi}_{mj}(r,z)\cdot\mathbf{\Phi}^*_{mj}(r,z) r\,\mathrm{d}r\,\mathrm{d}z \tag{26b}$$

$\mathbf{\Phi}^*_{mj}(r,z)$ is the complex conjugate of the eigenfunction. Unlike the elastic case where for each eigenfunction the eigenvalue pair is $+\omega_{mj}$ and $-\omega_{mj}$, in the visco-elastic case the pair is $+\omega_{mj}$ and $-\omega^*_{mj}$ where $(\ )^*$ stands for complex conjugate. This means that $\omega_{1mj} = \omega_{\mathrm{R}mj} + \mathrm{i}\omega_{\mathrm{I}mj}$ and $\omega_{2mj} = -\omega_{\mathrm{R}mj} + \mathrm{i}\omega_{\mathrm{I}mj}$. The reason $\omega_{\mathrm{I}mj}$ retains the same sign for both solutions is that $\omega_{\mathrm{I}mj}$ is a measure of damping which reduces amplitude whether the real part is $+\omega_{\mathrm{R}mj}$ or $-\omega_{\mathrm{R}mj}$. Consequently Eq. (21a) takes the form

$$\left(\frac{\mathrm{d}}{\mathrm{d}t} - \mathrm{i}\omega_{mj}\right)\left(\frac{\mathrm{d}}{\mathrm{d}t} + \mathrm{i}\omega^*_{mj}\right)a_{mjk}(t) = \bar{f}_{mjk}(t) \Rightarrow \left[\frac{\mathrm{d}^2}{\mathrm{d}t^2} + \mathrm{i}(\omega^*_{mj} - \omega_{mj})\frac{\mathrm{d}}{\mathrm{d}t} + \omega_{mj}\omega^*_{mj}\right]a_{mjk}(t) = \bar{f}_{mjk}(t) \tag{27}$$

Noting that $\mathrm{i}(\omega^*_{mj} - \omega_{mj}) = 2\omega_{\mathrm{I}mj}$ and $\omega_{mj}\omega^*_{mj} = \omega^2_{\mathrm{R}mj} + \omega^2_{\mathrm{I}mj}$, (27) simplifies to

$$\left[\frac{\mathrm{d}^2}{\mathrm{d}t^2} + 2\omega_{\mathrm{I}mj}\frac{\mathrm{d}}{\mathrm{d}t} + \omega^2_{\mathrm{R}mj} + \omega^2_{\mathrm{I}mj}\right]a_{mjk}(t) = \bar{f}_{mjk}(t) \tag{28}$$

Clearly, $\omega_{\mathrm{I}mj}$ acts as a velocity proportional viscous damper. Rewriting (28) in standard form:

$$\left[\frac{\mathrm{d}^2}{\mathrm{d}t^2} + 2\zeta_{mj}\bar{\omega}_{mj}\frac{\mathrm{d}}{\mathrm{d}t} + \bar{\omega}^2_{mj}\right]a_{mjk}(t) = \bar{f}_{mjk}(t); \quad \zeta_{mj} = \frac{\omega_{\mathrm{I}mj}}{\bar{\omega}_{mj}}; \quad \bar{\omega}_{mj} = \sqrt{\omega^2_{\mathrm{R}mj} + \omega^2_{\mathrm{I}mj}} \tag{29}$$

yields a solution in terms of a *Duhamel* integral:

$$\begin{aligned} a_{mjk}(t) &= -\frac{1}{\hat{\omega}_{mj}}\int_0^t \mathrm{e}^{-\zeta_{mj}\bar{\omega}_{mj}(t-\tau)}\sin\hat{\omega}_{mj}(t-\tau)\bar{f}_{mjk}(\tau)\,\mathrm{d}\tau \\ \hat{\omega}_{mj} &= \bar{\omega}_{mj}\sqrt{1-\zeta^2_{mj}} \end{aligned} \tag{30}$$

The general constitutive law for a linear viscoelastic material takes the form (see Fung (1965, pp. 416–418))

$$\sum_{n=0}^{N_\varepsilon}\tau_{\varepsilon n}\frac{\partial^n\sigma}{\partial t^n} = E_\mathrm{o}\sum_{n=0}^{N_\sigma}\tau_{\sigma n}\frac{\partial^n\varepsilon}{\partial t^n}, \quad \tau_{\sigma 0} = \tau_{\varepsilon 0} = 1 \tag{31}$$

$\tau_{\sigma n}$, $\tau_{\varepsilon n}$ are constants and E_o is a modulus. For a sinusoidal time dependence, (31) assumes the form of a *Padé* series

$$\begin{aligned} \sigma &= \beta_\tau(N_\sigma, N_\varepsilon;\omega)E_\mathrm{o}\varepsilon \\ \beta_\tau(N_\sigma, N_\varepsilon;\omega) &= \sum_{n=0}^{N_\sigma}\tau_{\sigma n}(\mathrm{i}\omega)^n \Big/ \sum_{n=0}^{N_\varepsilon}\tau_{\varepsilon n}(\mathrm{i}\omega)^n \end{aligned} \tag{32}$$

$\beta_\tau(N_\sigma, N_\varepsilon;\omega)$ is a complex valued function of ω. The simplest linear visco-elastic solid limits N_σ and N_ε to 1 reducing (32) to

$$\sigma = \frac{(1+\tau_{\sigma 1}\mathrm{i}\omega)}{(1+\tau_{\varepsilon 1}\mathrm{i}\omega)}E_\mathrm{o}\varepsilon \equiv \beta_\tau(1,1;\omega)E_\mathrm{o}\varepsilon \tag{33}$$

For the constitutive law in (33), approximations to ω_R and ω_I in (26a) are

$$\omega_R \approx \omega_o\left|\beta_\tau^{1/2}(1,1;\omega_{co})\right|, \quad \omega_I \approx \omega_o \mathrm{Im}\left(\beta_\tau^{1/2}(1,1;\omega_{co})\right)$$
$$\omega_{co} = \omega_{Ro} + i\omega_{Io} = \omega_o\left[\left|\beta_\tau^{1/2}(1,1;\omega_o)\right| + i\mathrm{Im}\left(\beta_\tau^{1/2}(1,1;\omega_o)\right)\right] \tag{34}$$

ω_o is the eigenfrequency of the linear elastic problem.

2. Results

In all results to follow, geometric and material properties of the cylinder are listed in Table 1. Fig. 1(a1) plots the static deformed generator from a unit radial displacement prescribed at the footprint

$$u_{so}(r_p, z) = H(z - z_a) - H(z - z_b) \tag{35a}$$

In (35a) $z_a = 1.5''$ and $z_b = 2.5''$. The resulting normalized $\sigma_{rrs}(r_p, z)$ distribution plotted in Fig. 1(b1) shows a rise near z_a and z_b of 1.5 times its magnitude at the plateau. Fig. 1(a2) and (b2) plot static deformed generator and normalized $\sigma_{rrs}(r_p, z)$ distribution for a unit axial displacement prescribed at the footprint

$$w_{so}(r_p, z) = H(z - z_a) - H(z - z_b) \tag{35b}$$

In this case, σ_{rrs} rises near z_a and z_b to 1.7 times its magnitude at the plateau.

Fig. 2(a) and (b) plots resonant frequency Ω in Hertz versus m with k_r as parameter for the two problems. The two spectra are almost identical for all m and k_r.

In Eq. (23), influence coefficients U_{lk} and W_{lk} require an approximation to the time dependence of the forcing pressure $f_p(t)$. One approximation is determined from the plane-strain state when axial length of cylinder and footprint approaches infinity (Appendix C). Fig. 3(a)–(d) plot histories of the plane-strain problem when a constant velocity $U_o = 330$ m/s is prescribed at $r = r_p$. There, u history shown as solid line in Fig. 3(a) reproduces the prescribed u_o profile. At $r = 2r_p$ and $r = 4r_p$, u histories exhibit the time-delay in wave front from propagation with finite speed c_ε. The closeness in magnitude of peak σ_{rr}, $\sigma_{\theta\theta}$ and σ_{zz} (Fig. 3(b)–(d)) implies a hydrodynamic state of stress. Geometric stress attenuation along r is proportional to $r^{-1/2}$.

The $\sigma_{rr}(r_p)$ plane-strain history in Fig. 3(b) serves as the approximation to $f_p(t)$ in the 3-D axisymmetric model as it is the limit when projectile and cylinder lengths are the same. Fig. 4(a1)–(d1) plots histories from the prescribed uniform pressure profile $f_p(t)$ at the center of the footprint $z = 2''$. The u history in Fig. 4(a1) does not follow the prescribed u_o profile because applied pressure is uniform over the footprint. Applying the influence method of Section 2 yields the histories in Fig. 4(a2)–(d2). The $u(r_p)$ history in Fig. 4(a2) matches the prescribed u_o profile. At the footprint, except for the higher stress peaks, results from prescribed velocity agree with those from the prescribed plane-strain pressure profile $f_p(t)$. At $r > r_p$, results

Table 1
Cylinder properties

E (lb/in^2)	4.5×10^4
ρ (lb s^2/in^4)	8.7×10^{-5}
v	0.48
l (in)	4
r_p (in)	0.25
r_o (in)	3
c_d (in/s)	6.74×10^4
c_s (in/s)	1.322×10^4

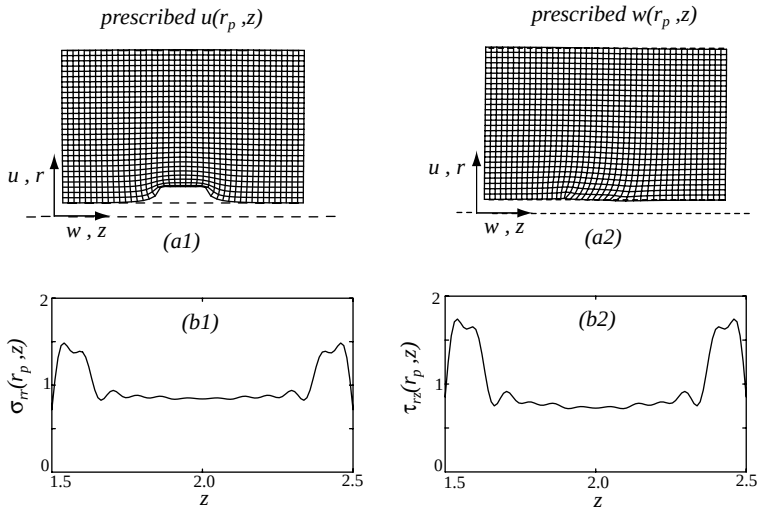

Fig. 1. Static deformation and foot-print traction at $r = r_p$, $z_a < z < z_b$ (a1), (b1) prescribed $u(r_p, z)$, (a2), (b2) prescribed $w(r_p, z)$.

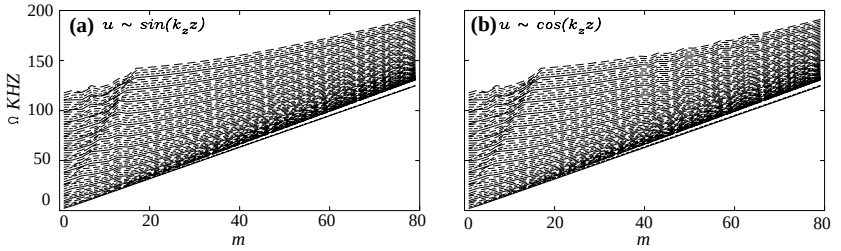

Fig. 2. Frequency spectra (a) radial problem, $u \sim \sin(k_z z)$, (b) axial problem, $u \sim \cos(k_z z)$.

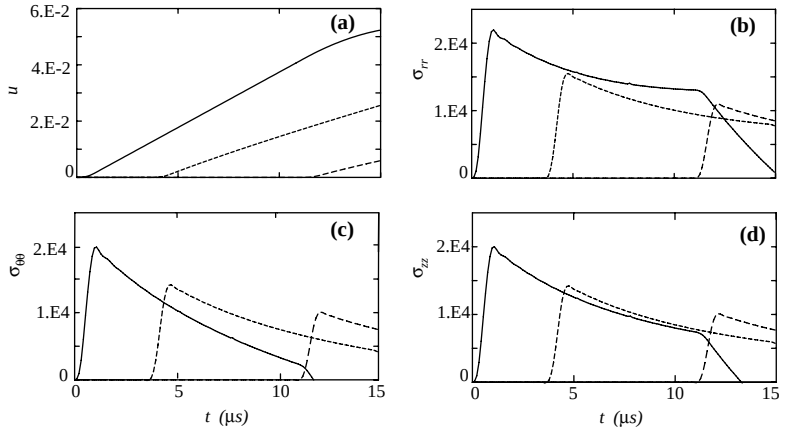

Fig. 3. Plane-strain histories from prescribed radial velocity (—) $r = r_p$, (- - -) $r = 2r_p$, (– – –) $r = 4r_p$; (a) u, (b) σ_{rr}, (c) $\sigma_{\theta\theta}$, (d) σ_{zz}.

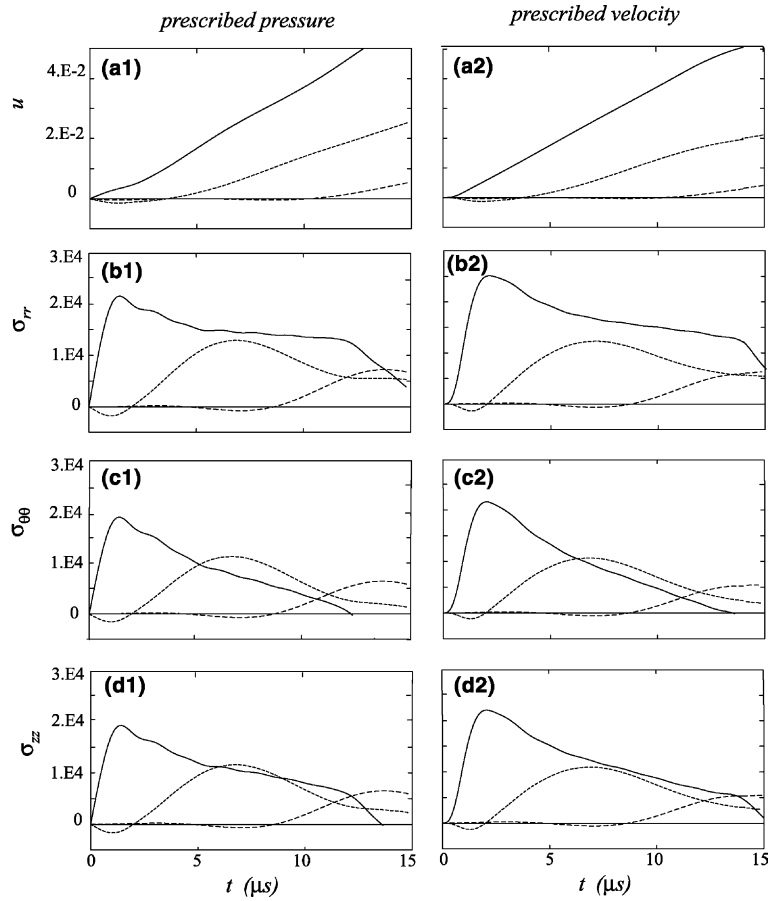

Fig. 4. Histories from radial excitation at $z = 2''$ (—) $r = r_p$, (- - -) $r = 2r_p$, (– – –) $r = 4r_p$; (a1), (b1), (c1), (d1) prescribed pressure from plane-strain (a2), (b2), (c2), (d2) prescribed velocity.

from the two forcing methods coincide implying that the plane-strain pressure profile is a good approximation to the actual profile determined by the influence method. Geometric stress attenuation along r is proportional to $r^{-3/4}$. Fig. 5(a)–(d) plots histories from prescribed velocity remote from the footprint at $z = 2.6''$. There, peak normal stresses are 1/5 those under the footprint (see Fig. 4(b2), (c2) and (d2)). This steep drop in stress across the edges of the footprint is caused by the low shear rigidity of the material consistent with the ratio $c_s/c_d \simeq 1/5$ from Table 1.

Fig. 6 plots instantaneous $\sigma_{rr}(r_p, z; t_0)$ distributions for 2 μs $\leqslant t_0 \leqslant$ 12 μs in intervals of 2 μs. For $t_0 = 2$ μs, the distribution is parabolic with a maximum at the center of the footprint. As time increases, the distribution becomes flatter then develops peaks near z_a and z_b resembling the static case in Fig. 1(b1). The step-like shape of the distribution is an artifact of the finite number of pressure ring segments dividing the footprint. In Fig. 6, the 8 steps correspond to 8 ring segments. The distribution becomes smoother as number of ring segments increases.

For an axial prescribed velocity at $r = r_p$ along $z_a \leqslant z \leqslant z_b$, the approximation to $f_p(t)$ is determined from the solution of the pure-shear problem of an infinite cylinder with axial velocity prescribed at $r = r_p$ derived in Appendix D. Fig. 7(a) and (b) plots histories of w and τ_{rz} for the case of pure shear. Since $c_s/c_d = 1/5$, the time range in these histories is extended to 40 μs to allow for the longer arrival time at stations remote from

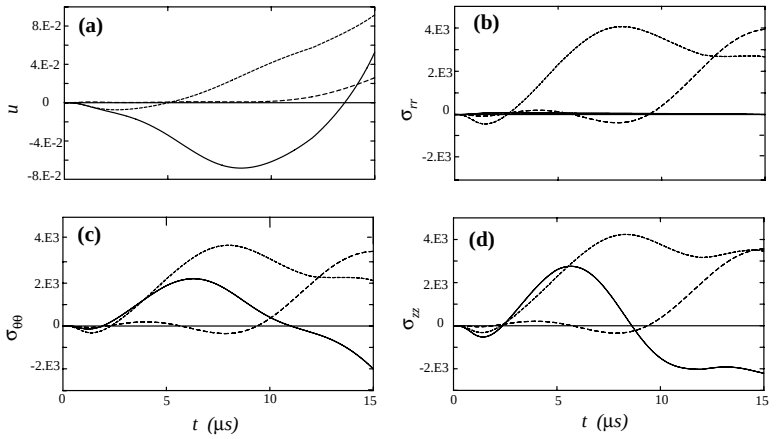

Fig. 5. Histories from prescribed radial velocity at $z = 2.6''$ (—) $r = r_p$, (- - -) $r = 2r_p$, (– – –) $r = 4r_p$; (a) u, (b) σ_{rr}, (c) $\sigma_{\theta\theta}$, (d) σ_{zz}.

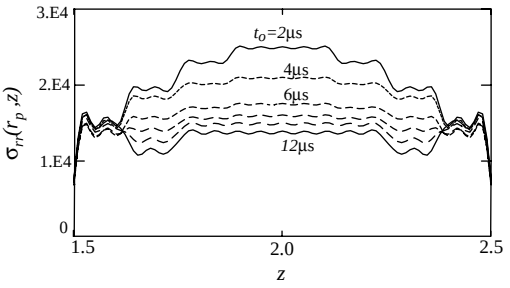

Fig. 6. Instantaneous $\sigma_{rr}(r_p, z; t_0)$ distribution over footprint from prescribed radial velocity.

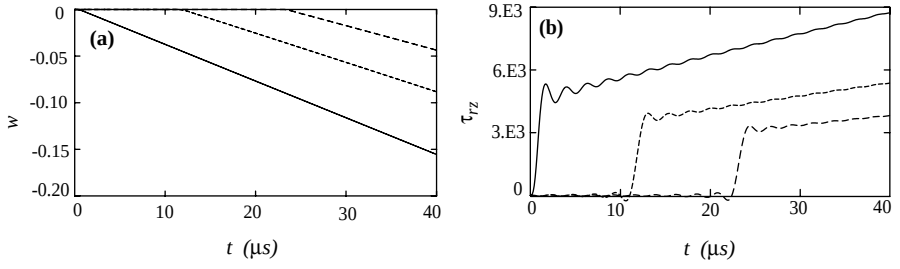

Fig. 7. Pure-shear histories from prescribed axial velocity (—) $r = r_p$, (- - -) $r = 1.6r_p$, (– – –) $r = 2.2r_p$; (a) w, (b) τ_{rz}.

the footprint. The τ_{rz} profile in Fig. 7(b) is then used as an approximation $f_p(t)$ in computing histories with prescribed velocity.

Fig. 8(a1) and (b1) plots histories at the center of the footprint $z = 2''$ from a uniform $\tau_{rzo}(r_p, z, t) = f_p(t)$ prescribed over the footprint. Fig. 8(a1) shows that $\partial_t w$ is the same as prescribed velocity $U_0 = 330$ ft/s till $t = 10$ μs, then diminishes to 200 ft/s near $t = 40$ μs. On the other hand for prescribed velocity, $\partial_t w$ in Fig. 8(b2) is constant for all times and equals U_o. Magnitude of τ_{rz} in Fig. 8(b2) is higher than that in Fig. 8(b1) by approximately a factor of 1.3.

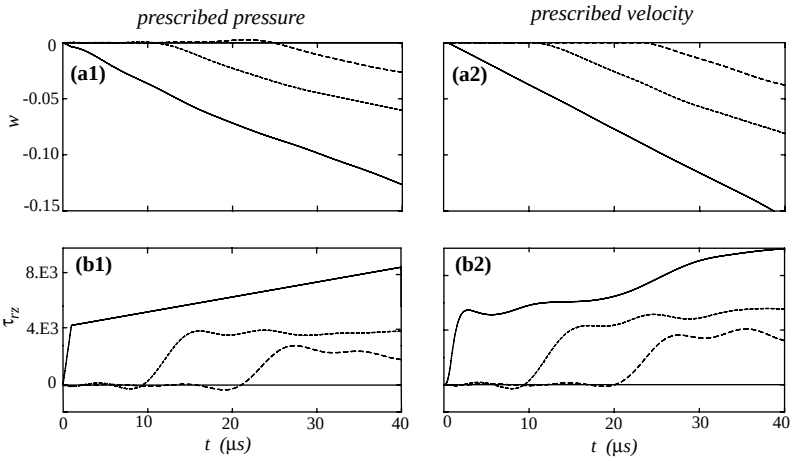

Fig. 8. Histories from axial excitation at $z = 2''$ (—) $r = r_p$, (- - -) $r = 1.6r_p$, (– – –) $r = 2.2r_p$; (a1), (b1), prescribed pressure from pure-shear; (a2), (b2), prescribed velocity.

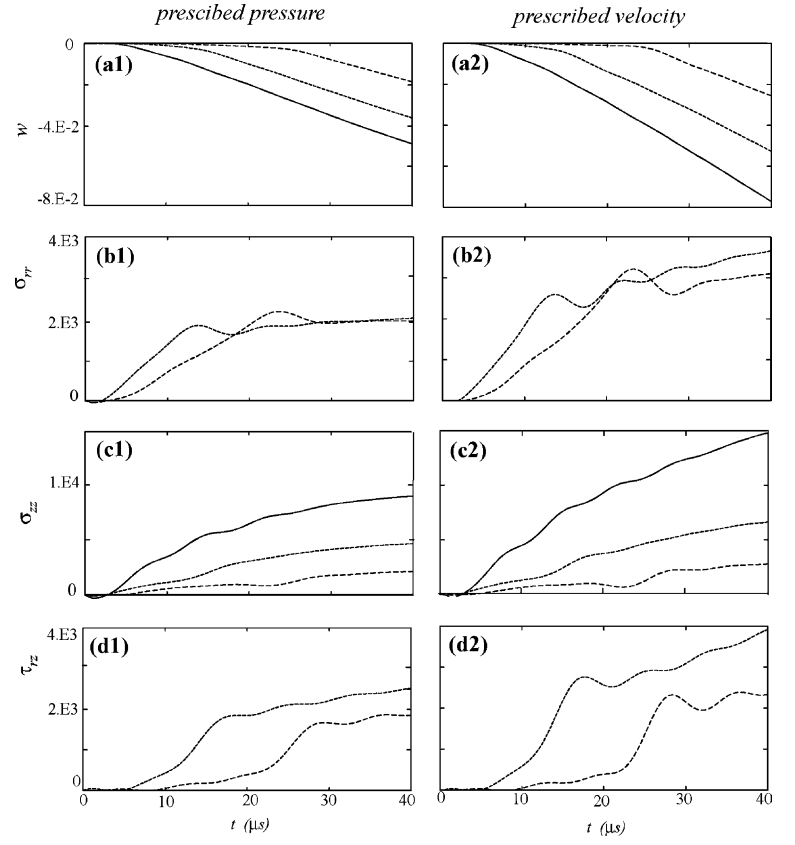

Fig. 9. Histories from axial excitation at $z = 2.6''$ (—) $r = r_p$, (- - -) $r = 1.6r_p$, (– – –) $r = 2.2r_p$; (a1) w, (b1) σ_{rr}, (c1) σ_{zz}, (d1) τ_{rz} prescribed pressure from pure-shear; (a2) w, (b2) σ_{rr}, (c2) σ_{zz}, (d2) τ_{rz} prescribed velocity.

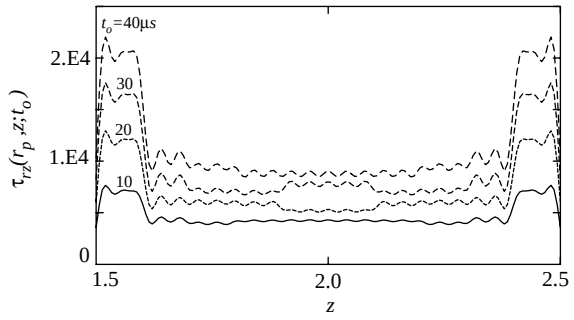

Fig. 10. Instantaneous $\tau_{rz}(r_p, z; t_0)$ distribution over footprint from prescribed axial velocity.

Remote from the footprint at $z = 2.6''$, histories with prescribed pressure (Fig. 9(a1)–(d1)) are compared to those with prescribed velocity (Fig. 9(a2)–(d2)). In Fig. 9(a1)–(d1) all variables are approximately half the corresponding variables in Fig. 9(a2)–(d2). Fig. 10 plots τ_{rz} distribution along the footprint. For $t_0 < 10$ μs, τ_{rz}'s distribution is uniform. As time increases, τ_{rz} rises steeply near the edges of the footprint reaching a value double its value at the center at $t_0 \approx 40$ μs.

3. Conclusion

Wave propagation in a hollow cylinder is analyzed for pressure and velocity prescribed at its inner boundary. The difficulty arising from the mixed boundary conditions is overcome by the influence coefficient method. An approximation to the prescribed pressure profile needed in this method is determined from the plane-strain solution. Noteworthy results are

(1) The stress state close to impact is almost hydrodynamic.
(2) Results from prescribed radial velocity agree with those from prescribed uniform pressure determined from the plane-strain model.
(3) In the plane-strain model, stress attenuation along r follows $r^{-1/2}$ while in the 3-D axisymmetric model it follows $r^{-3/4}$.
(4) For prescribed radial velocity, the instantaneous σ_{rr} distribution is parabolic soon after impact, and approaches the static distribution for large times.
(5) Near the center of the footprint, results from prescribed axial velocity agree with those from prescribed uniform shear stress determined from the pure-shear model. However, near the edges of the footprint, stresses from prescribed pressure are half of those from prescribed velocity because in the later τ_{rz} rises near the edges by the same factor.

Appendix A. Static problem

In what follows, all dependent variables pertaining to the static solution will be subscripted by s. The static axisymmetric equations in terms of displacements are

$$\begin{aligned}
&\left((\lambda+2\mu)\widehat{\nabla}_1^2+\mu\partial_{zz}\right)u_s+(\lambda+\mu)\partial_{rz}w_s=0\\
&(\lambda+\mu)\partial_z(\partial_r+1/r)u_s+(\mu\widehat{\nabla}_0^2+(\lambda+2\mu)\partial_{zz})w_s=0\\
&\widehat{\nabla}_n^2\equiv\partial_{rr}+1/r\partial_r-n^2/r^2,\quad n=0,1
\end{aligned}\tag{A.1}$$

Eq. (A.1) decouple to

$$\begin{aligned}&\mu(\lambda+2\mu)(\widehat{\nabla}_1^2+\partial_{zz})^2u_{\mathrm{s}}=0\\&\mu(\lambda+2\mu)(\widehat{\nabla}_0^2+\partial_{zz})^2w_{\mathrm{s}}=0\end{aligned}\tag{A.2}$$

For the radial traction problem satisfying $\sigma_{zzs}=0$ at $z=(0,l)$, separation of variables follows Eq. (11) in the text. Summing over all k_z yields

$$u_{\mathrm{s}}(r,z)=\sum_{m=1}^{M}\bar{u}_{m\mathrm{s}}(r)\sin(k_{zm}z)\tag{A.3a}$$

$$w_{\mathrm{s}}(r,z)=\sum_{m=1}^{M}\bar{w}_{m\mathrm{s}}(r)\cos(k_{zm}z),\quad k_{zm}=m\pi/l\tag{A.3b}$$

Substituting (A.3) in (A.2) produces uncoupled equations in r for each k_{zm}

$$\begin{aligned}&(\widehat{\nabla}_1^2-k_{zm}^2)^2\bar{u}_{m\mathrm{s}}(r)=0\\&(\widehat{\nabla}_0^2-k_{zm}^2)^2\bar{w}_{m\mathrm{s}}(r)=0\end{aligned}\tag{A.4}$$

In what follows, subscript m will be dropped for shortness. Eq. (A.4) admit the solutions

$$\bar{u}_{\mathrm{s}}(r)=C_1I_1(k_zr)+C_2K_1(k_zr)+C_3(k_zrI_0(k_zr)-I_1(k_zr))-C_4(k_zrK_0(k_zr)+K_1(k_zr))\tag{A.5a}$$

$$\begin{aligned}&\bar{w}_{\mathrm{s}}(r)=C_1I_0(k_zr)-C_2K_0(k_zr)+C_3(\alpha_1I_0(k_zr)+k_zrI_1(k_zr))+C_4(-\alpha_1K_0(k_zr)+k_zrK_1(k_zr))\\&\alpha_1=(\lambda+3\mu)/(\lambda+\mu),\quad\alpha_2=\lambda/(\lambda+\mu)\end{aligned}\tag{A.5b}$$

Substituting (A.5a) and (A.5b) in the constitutive relations (14) and (15a) of the text yields

$$\begin{aligned}\bar{\sigma}_{rrs}(r)=&\,2\mu k_z(C_1(I_0(k_zr)-I_1(k_zr)/(k_zr))-C_2(K_0(k_zr)+K_1(k_zr)/(k_zr)))\\&+2\mu k_zC_3(-\alpha_2I_0(k_zr)+(1+(k_zr)^2)I_1(k_zr)/(k_zr))+2\mu k_zC_4(\alpha_2K_0(k_zr)+(1+(k_zr)^2)K_1(k_zr)/(k_zr))\end{aligned}\tag{A.6a}$$

$$\begin{aligned}\bar{\sigma}_{\theta\theta\mathrm{s}}(r)=&\,2\mu k_z(C_1I_1(k_zr)/(k_zr)+C_2K_1(k_zr)/(k_zr))+2\mu k_zC_3((1-\alpha_2)I_0(\mathrm{i}k_zr)-I_1(k_zr)/(k_zr))\\&+2\mu k_zC_4(-(1-\alpha_2)K_0(k_zr)-K_1(k_zr)/(k_zr))\end{aligned}\tag{A.6b}$$

$$\begin{aligned}\bar{\sigma}_{zzs}(r)=&\,2\mu k_z(-C_1I_0(k_zr)+C_2K_0(k_zr))+2\mu k_zC_3(-(\alpha_1+\alpha_2)I_0(k_zr)-k_zrI_1(k_zr))\\&+2\mu k_zC_4((\alpha_1+\alpha_2)K_0(k_zr)-k_zrK_1(k_zr))\end{aligned}\tag{A.6c}$$

$$\begin{aligned}\bar{\tau}_{rzs}(r)=&\,2\mu k_z(C_1I_1(k_zr)+C_2K_1(k_zr))+2\mu k_zC_3(k_zrI_0(k_zr)+(1-\alpha_2)I_1(k_zr))\\&+2\mu k_zC_4(-k_zrK_0(k_zr)+(1-\alpha_2)K_1(k_zr))\end{aligned}\tag{A.6d}$$

Tractions at the inner and outer surfaces of the tube are expressed as

$$\begin{aligned}&\sigma_{rrs}(r_{\mathrm{p}},z)=p_r(H(z-z_a)-H(z-z_b))\\&\tau_{rzs}(r_{\mathrm{p}},z)=0\end{aligned}\tag{A.7a}$$

$$\sigma_{rrs}(r_{\mathrm{o}},z)\equiv\tau_{rzs}(r_{\mathrm{o}},z)=0\tag{A.7b}$$

p_r is a uniform radial traction prescribed at $r=r_{\mathrm{p}}$ in the interval $z_a\leqslant z\leqslant z_b$. Substituting (A.6a) and (A.6d) in (A.7a) and (A.7b) and enforcing orthogonality of $\sin(k_zz)$ and $\cos(k_zz)$ produces M (4×4) uncoupled matrix equations in the coefficients C_{km}, $k=1,4$

$$\mathbf{M}_{cm}\mathbf{C}_m = \mathbf{f}_m \tag{A.8}$$

Coefficients of $\mathbf{M}_{cm}$ are the radial functions multiplying C_{km} in (A.6a) and (A.6d) evaluated at $r = r_p$ and $r = r_o$, and $\mathbf{f}_m$ is a vector defined by

$$\begin{aligned} f_{1m} &= -2p_r(\cos(k_{zm}z_b) - \cos(k_{zm}z_a))/(k_{zm}l) \\ f_{2m} &\equiv f_{3m} \equiv f_{4m} = 0 \end{aligned} \tag{A.9}$$

For the axial traction problem satisfying vanishing shear stress $\tau_{rzs} = 0$ at $z = (0, l)$, the expansion in (A.3) becomes

$$\begin{aligned} u_s(r,z) &= \sum_{m=1}^{M} \bar{u}_{ms}(r)\cos(k_{zm}z) \\ w_s(r,z) &= \sum_{m=1}^{M} \bar{w}_{ms}(r)\sin(k_{zm}z), \quad k_{zm} = m\pi/l \end{aligned} \tag{A.10}$$

The boundary conditions are

$$\begin{aligned} &\tau_{rzs}(r_p, z) = 0 \\ &\sigma_{rrs}(r_p, z) = p_r(H(z - z_a) - H(z - z_b)) \end{aligned} \tag{A.7a}$$

$$\sigma_{rrs}(r_o, z) \equiv \tau_{rzs}(r_o, z) = 0 \tag{A.7b}$$

p_z is a uniform axial traction applied at $r = r_p$ in the interval $z_a \leqslant z \leqslant z_b$. Expressions for displacements and stresses resemble those of the radial problem and are omitted here for shortness.

Appendix B. Modal analysis

The dynamic solution $\mathbf{u}_d(r, z, t)$ satisfies the homogeneous boundary conditions

$$\begin{aligned} &\sigma_{rr}(r_p, z, t) = 0, \quad \tau_{rz}(r_p, z, t) = 0 \\ &\sigma_{rr}(r_o, z, t) = 0, \quad \tau_{rz}(r_o, z, t), = 0 \end{aligned} \tag{B.1}$$

Substituting (16a) and (16d) in (B.1) yields the matrix equation

$$\mathbf{M}_e\mathbf{C} = 0 \tag{B.2}$$

$\mathbf{M}_e$ is a 4×4 square matrix, $\mathbf{C} = \{C_1, C_2, C_3, C_4\}^T$ is the vector of unknown coefficients and

$$\begin{aligned} M_{e11} &= -((\lambda + 2\mu)k_e^2 + \lambda k_z^2)J_0(k_e r_p) + 2\mu k_e^2 J_1(k_e r_p)/(k_e r_p) \\ M_{e13} &= 2\mu k_s k_z [J_0(k_s r_p) - J_1(k_s r_p)/(k_s r_p)] \\ M_{e21} &= -2\mu k_e k_z J_1(k_e r_p) \\ M_{e23} &= -\mu(k_s^2 - k_z^2)J_1(k_s r) \end{aligned} \tag{B.3}$$

M_{e12}, M_{e14}, M_{e22}, M_{e24} have the same form as M_{e11}, M_{e13}, M_{e21}, M_{e23} with J_n replaced by Y_n. Similarly, M_{e3k}, M_{e4k} $k = 1, 4$ have the same form as M_{e1k}, M_{e2k} $k = 1, 4$, with r_p replaced by r_o. From the definitions of k_e and k_s in (12), k_e is imaginary when $\omega < k_z c_d$, $c_d = \sqrt{(\lambda + 2\mu)/\rho}$, and k_s is imaginary when $\omega < k_z c_s$, $c_s = \sqrt{\mu/\rho}$. Below these cut-off frequencies, J_n and Y_n are replaced by I_n and K_n with appropriate changes in sign. For each m in k_z, a non- trivial solution to (B.2) yields the implicit eigenvalue problem

$$\det|M_{em}| = 0 \Rightarrow \{\omega_{mj}; \mathbf{\Phi}_{mj}(r, z)\} \tag{B.4}$$

$\{\omega_{mj}; \mathbf{\Phi}_{mj}(r, z)\}$ is the eigen-dyad corresponding to the mth axial wave-number.

Appendix C. Plane-strain problem

The radial plane-strain problem is that of an infinite hollow cylinder where $\varepsilon_{zz} \equiv w \equiv \partial_z \equiv 0$. The dynamic equation in u then reduces to

$$\begin{aligned} &\widehat{\nabla}_1^2 u = 1/c_\varepsilon^2 \partial_{tt} u, \quad r_\mathrm{p} \leqslant r \leqslant r_\mathrm{o} \\ &\widehat{\nabla}_1^2 \equiv \partial_{rr} + 1/r\partial_r - 1/r^2, \quad c_\varepsilon^2 = E_\varepsilon/\rho \\ &E_\varepsilon = E(1-\nu)/((1+\nu)(1-2\nu)) \end{aligned} \tag{C.1}$$

The boundary conditions are

$$u(r_\mathrm{p}, t) = f_p(t), \quad \sigma_{rr}(r_\mathrm{o}, t) = 0 \tag{C.2}$$

$f_p(t)$ is the time dependent displacement profile prescribed at $r = r_\mathrm{p}$. The constitutive law takes the form

$$\begin{aligned} &\sigma_{ii} = \lambda \varepsilon_V + 2\mu \varepsilon_{ii}, \quad ii \to rr, \theta\theta, zz \\ &\varepsilon_V = \varepsilon_{rr} + \varepsilon_{\theta\theta}, \quad \varepsilon_{zz} \equiv 0 \end{aligned} \tag{C.3a}$$

$$\begin{aligned} &\sigma_{rr} = E_\varepsilon(\partial_r u + \nu/(1-\nu)u/r) \\ &\sigma_{\theta\theta} = E_\varepsilon(u/r + \nu/(1-\nu)\partial_r u) \\ &\sigma_{zz} = E_\varepsilon(u/r + \partial_r u)\nu/(1-\nu) \end{aligned} \tag{C.3b}$$

Express $u(r,t)$ as a superposition of a static and a dynamic solution

$$u(r,t) = u_s(r) f_p(t) + u_\mathrm{d}(r,t) \tag{C.4}$$

$u_\mathrm{s}(r)$ is the static solution satisfying the inhomogeneous boundary conditions

$$u_\mathrm{s}(r_\mathrm{p}) = 1, \quad \sigma_{rrs}(r_\mathrm{o}) = 0 \tag{C.5}$$

$u_\mathrm{d}(r,t)$ is the dynamic solution satisfying the homogeneous form of boundary conditions (C.2). Expand $u_\mathrm{d}(r,t)$ in the eigenfunctions $\varphi_j(r)$ of (C.1)

$$\begin{aligned} &u_\mathrm{d}(r,t) = \sum_j a_j(t)\varphi_j(r) \\ &\varphi_j(r) = J_1(k_{rj}r) + c_2 Y_1(k_{rj}r), \quad c_2 = -J_1(k_{rj}r_\mathrm{p})/Y_1(k_{rj}r_\mathrm{p}) \end{aligned} \tag{C.6}$$

Substituting (C.6) in the homogeneous form of (C.2) yields the dispersion relation

$$\begin{aligned} &\alpha_{11}\alpha_{22} - \alpha_{12}\alpha_{21} = 0 \\ &\alpha_{11} = J_1(k_{rj}r_\mathrm{p}), \quad \alpha_{12} = Y_1(k_{rj}r_\mathrm{p}) \\ &\alpha_{21} = (\lambda + 2\mu)k_{rj}J_1'(k_{rj}r_\mathrm{o}) + \lambda J_1(k_{rj}r_\mathrm{o})/r_\mathrm{o} \\ &\alpha_{22} = (\lambda + 2\mu)k_{rj}Y_1'(k_{rj}r_\mathrm{o}) + \lambda Y_1(k_{rj}r_\mathrm{o})/r_\mathrm{o} \end{aligned} \tag{C.7}$$

$(\ )'$ stands for derivative with respect to the argument. (C.7) determines the wave numbers k_{rj}. The static solution to $\nabla_1^2 u_s = 0$ is

$$\begin{aligned} &u_s(r) = Ar + B/r \\ &A = r_\mathrm{p}(r_\mathrm{p}^2 + (\lambda+\mu)r_\mathrm{c}^2/\mu)^{-1}, \ B = r_\mathrm{p}(1 - Ar_\mathrm{p}) \end{aligned} \tag{C.8}$$

The constitutive law is given by (C.3b). Substituting (C.6) and (C.8) in (C.4) and enforcing orthogonality of $\varphi_j(r)$ yields

$$\ddot{a}_j(t) + \omega_j^2 a_j(t) = -(N_{aj}/N_{jj})\ddot{f}_p(t)$$
$$N_{jj} = \int_{r_p}^{r_o} \varphi_j^2(r) r\,\mathrm{d}r, \quad N_{aj} = \int_{r_p}^{r_o} u_s(r)\varphi_j(r) r\,\mathrm{d}r, \quad \omega_j = c_d k_{rj} \tag{C.9}$$

$(\cdot)$ stands for time derivative. The integrals in N_{jj} and N_{aj} are evaluated analytically in terms of J_n and Y_n for $n = 0, 1, 2$.

For the radial plane-stress problem, $\sigma_{zz} \equiv w \equiv \partial_z \equiv 0$ yielding the equation

$$\widehat{\nabla}_1^2 u = 1/c_\sigma^2 \partial_{tt} u, \quad \widehat{\nabla}_1^2 \equiv \partial_{rr} + 1/r\partial_r - 1/r^2$$
$$c_\sigma^2 = E/(\rho(1-\nu^2)), \quad r_p \leqslant r \leqslant r_c \tag{C.10}$$

(C.10) has the same form as (C.1) but with a lower speed of propagation since $c_\sigma/c_d = (1-2\nu)^{1/2}/(1-\nu)$ is small when ν is close to 1/2. The constitutive law simplifies to

$$\sigma_{rr} = E_\sigma(\partial_r u + \nu u/r), \quad \sigma_{\theta\theta} = E_\sigma(u/r + \nu\partial_r u)$$
$$\sigma_{zz} = 0, \quad E_\sigma = E/(1-\nu^2) \tag{C.11}$$

If prescribed displacement at $r = r_p$ is the same for both plane stress and plane strain, then strains are approximately the same. It follows that stresses in (C.11) are smaller than those in (C.3b) by a factor of $(c_\sigma/c_d)^2$. In the present application, if material of the cylinder fails radially within the footprint $z_a \leqslant z \leqslant z_b$, then the approximate state of plane-strain changes to that of plane-stress reducing transmitted pressure substantially.

Appendix D. Pure shear problem

For the pure shear problem, $\sigma_{rr} \equiv \sigma_{\theta\theta} \equiv \sigma_{zz} \equiv u \equiv 0$ yielding the equation

$$\widehat{\nabla}_0^2 w = 1/c_s^2 \partial_{tt}^2 w, \quad \widehat{\nabla}_0^2 = \partial_{rr} + 1/r\partial_r$$
$$c_s^2 = E/(2\rho(1+\nu)), \quad r_p \leqslant r \leqslant r_o \tag{D.1a}$$

$$w(r_p, t) = f_p(t), \quad \tau_{rz}(r_o, t) = 0 \tag{D.1b}$$

$$\tau_{rz}(r, t) = E/(2(1+\nu))\partial_r w(r, t) \tag{D.1c}$$

Express w as a superposition of a static and a dynamic solution

$$w(r, t) = w_s(r) f_p(t) + w_d(r, t) \tag{D.2a}$$

$$\widehat{\nabla}_0^2 w_s = 0, \quad w_s(r_p) = 1, \quad \tau_{rzs}(r_o) = 0 \tag{D.2b}$$

$$\widehat{\nabla}_0^2 w_d = 1/c_s^2 \partial_{tt} w_d, \quad w_d(r_p, t) = 0, \quad \tau_{rzd}(r_o, t) = 0 \tag{D.2c}$$

Since (D.2b) admits a rigid body motion, a body-force b_f is subtracted from (D.2b) so as to equilibrate the external shear traction and $b_f f_p(t)$ is added to (D.2c) to cancel its effect. This yields

$$\begin{aligned}\widehat{\nabla}_0^2 w_{\mathrm{s}} &= -b_f \\ \widehat{\nabla}_0^2 w_{\mathrm{d}} &= 1/c_{\mathrm{s}}^2 \partial_{tt}^2 w_{\mathrm{d}} + b_f f_p(t)\end{aligned} \tag{D.3}$$

The solution to w_{s} satisfying the boundary conditions (D.2b) is

$$\begin{aligned}w_{\mathrm{s}}(r) &= (2r_{\mathrm{o}}^2 \ln r - r^2)/(2r_{\mathrm{o}}^2 \ln r_{\mathrm{p}} - r_{\mathrm{p}}^2) \\ \tau_{rz\mathrm{s}}(r) &= \frac{E}{(1+v)} \frac{(r_{\mathrm{o}}^2 - r^2)}{(2r_0^2 \ln(r_{\mathrm{p}}) - r_{\mathrm{p}}^2) r} \\ b_f &= 2/(r_{\mathrm{o}}^2 \ln r_{\mathrm{p}} - r_{\mathrm{p}}^2/2)\end{aligned} \tag{D.4}$$

Expand w_{d} in terms of its eigenfunctions $\varphi_j(r)$

$$\begin{aligned}w_{\mathrm{d}}(r,t) &= \sum_j a_j(t)\varphi_j(r) \\ \varphi_j(r) &= J_0(k_{rj} r) - (J_0(k_{rj} r_{\mathrm{p}})/Y_0(k_{rj} r_{\mathrm{p}}))Y_0(k_{rj} r)\end{aligned} \tag{D.5}$$

Substituting (D.2a) in (D.1a) using (D.3) and (D.5) and enforcing the orthogonality of $\varphi_j(r)$ produces uncoupled equations in $a_j(t)$

$$\begin{aligned}&\ddot{a}_j(t) + \omega_j^2 a_j(t) = -(N_{aj}/N_{jj})\ddot{f}_p(t) - (N_{bj}/N_{jj}) c_{\mathrm{s}}^2 b_f f_p(t) \\ &N_{aj} = \int_{r_{\mathrm{p}}}^{r_{\mathrm{o}}} \varphi_j(r) w_{\mathrm{s}}(r) r\,\mathrm{d}r, \quad N_{bj} = \int_{r_{\mathrm{p}}}^{r_{\mathrm{o}}} \varphi_j(r) r\,\mathrm{d}r, \quad N_{jj} = \int_{r_{\mathrm{p}}}^{r_{\mathrm{o}}} \varphi_j^2(r) r\,\mathrm{d}r\end{aligned} \tag{D.6}$$

$(\cdot)$ is time derivative and ω_j are roots of the dispersion relation

$$J_0(k_{rj} r_{\mathrm{p}}) Y_0'(k_{rj} r_{\mathrm{o}}) - J_0'(k_{rj} r_{\mathrm{o}}) Y_0(k_{rj} r_{\mathrm{p}}) = 0, \quad k_{rj} = \omega_j / c_{\mathrm{s}} \tag{D.7}$$

$(\ )'$ is derivative with respect to the argument.

References

Bao, X. et al., 1997. The resonances of finite- length elastic cylinders and elastic spheroids excited by sound scattering. Journal of the Acoustical Society of America 102, 49.

Batard, H., Quentin, G., 1992. Acoustical resonances of solid elastic cylinders: Parametric study. Journal of the Acoustical Society of America 91, 581.

Cheung, Z., Lo, Y., Au, S., 2003. 3-D vibration analysis of solid and hollow circular cylinders via Chebyshev–Ritz method. Computer Methods in Applied Mechanics and Engineering 192, 13–14, 1575–1589.

Fung, Y.C., 1965. In: Foundations of solid mechanics, first ed. Prentice-Hall International Series in Dynamics. Prentice-Hall, Inc., Englewood Cliffs, NJ.

Grinchenko, V., 1999. Eigenforms and eigenfrequency spectrum of finite elastic cylinder. Journal of the Acoustical Society of America 105, 1392.

Grinchenko, V., Meleshko, V., 1978. Axisymmetric vibrations of an elastic cylinder of finite length. Soviet Physics Acoustics 24, 488.

Honarvar, F., Sinclair, A., 1996. Acoustic wave scattering from transversely isotroplic cylinders. Journal of the Acoustical Society of America 100, 57.

Hussein, M., Heyliger, P., 1998. Three-dimensional vibrations of layered piezoelectric cylinders. Journal of Engineering Mechanics 124, 1294.

Love, A.E., 1944. A treatise on the mathematical theory of elasticity, first American ed. Dover Publcations Inc., New York. pp. 287–292.

Paul, H., Murali, V., 1995. Dynamic response of axisymmetric poroelastic cylindrical bone. Journal of the Acoustical Society of America 98 (5), 2978.

Soldatos, K., 1994. Review of three-dimensional dynamic analyses of circular cylinders and cylindrical shells, American Society of Mechanical Engineers. Applied Mechanics Reviews 47 (10), 501–516.

Soldatos, K., Ye, J., 1994. Wave propagation in anisotropic laminated hollow cylinders of infinite extent. Journal of the Acoustical Society of America 96 (6), 3744–3752.

Stanton, T., 1988. Sound scattering by cylinders of finite length. II. Elastic cylinders. Journal of the Acoustical Society of America 83, 64.

Stepanishen, P., Janus, R., 1990. Transient radiation and scattering from fluid loaded elastic cylinders. Journal of the Acoustical Society of America 88 (Suppl. 1), S78.

Wang, X., Ying, C., 2001. Scattering of Lamb waves by a circular cylinder. Journal of the Acoustical Society of America 110, 1752.

Yin, X., Yue, Z., 2002. Transient plane-strain response of multilayered elastic cylinders to axisymmetric impulse. Journal of Applied Mechanics 69, 825.